ERRATA: REPLACE CHAPTER 28

28

Ultrasound Contrast Agents

MARK A. BORDEN, SHENGPING QIN, AND KATHERINE W. FERRARA

Due to its safety, portability, and low cost, ultrasound imaging is widely used for clinical applications spanning cardiology, peripheral vascular disease, obstetrics, kidney diseases and cancer. Ultrasound molecular imaging is becoming increasingly popular for small-animal studies, particularly those involving multiple imaging modalities. Ultrasonic blood echoes are ~two orders of magnitude smaller than tissue echoes due to the relatively small acoustic impedance difference between red blood cells and plasma. To detect small blood vessels and receptors within these vessels, ultrasonic contrast agents have been engineered, and each can be characterized as a biocolloid—a colloidal particle made from biocompatible materials. Several types of biocolloids have been used as ultrasound contrast agents, including gas-liquid emulsions (microbubbles), liquid-liquid emulsions (nanodrops), liposomes, and other particles. The degree of acoustic backscatter depends on the intrinsic properties of the biocolloid. The compressibility of the biocolloid and the density difference between the biocolloid and surrounding tissue contribute to the acoustic backscatter. Nonlinear effects and resonance can also contribute considerably to the echo response.

One advantage of the biocolloid is its payload capacity, making it amenable to multimodality imaging or the dual purposes of imaging and therapy (ie, "point and shoot"). Another is the surface area for targeting. Biocolloids range in size between 10 nm and 10 μm in diameter and therefore can be engineered to present many ligands. Multiple ligand-receptor interactions can lead to firm adhesion, even in the face of hydrodynamic forces acting to dislodge the biocolloid.

This chapter will introduce the biocolloids that are being used as contrast agents for ultrasound molecular imaging, with the structures and their typical sizes summarized in Figure 1. Emphasis is placed on the most popular and theoretically superior echo-contrast agent, the microbubble. Physicochemistry is covered because an understanding of structure-property relationships is the key to engineering and interpreting the performance of targeted ultrasound contrast agents. Interactions between the microbubble and ultrasound device are discussed in the context of methods used to exploit them for the purposes of molecular imaging. Details of ultrasound instrumentation, which is used to excite and detect microbubbles *in vivo*, are covered in Chapter 15, "Ultrasound".

We start by summarizing the properties of solid and liquid nanoparticles, and follow this discussion with a focus on microbubbles, which are favored for their ability to compress and expand with the passing ultrasound wave and produce distinct acoustic signatures that can be detected with high fidelity.

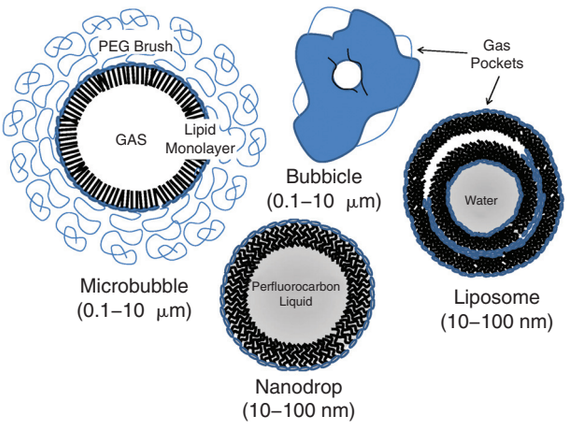

Figure 1. Cartoon representation of ultrasound contrast agents ranging from micron-sized bubbles to liposomes and nanodroplets with diameters as small as tens of nanometers.

SOLID AND LIQUID NANOPARTICLES

The commonly used ultrasound contrast agents include a class of submicron particles (nanoparticles) that are primarily composed of a solid or liquid. Solid and liquid nanoparticles tend to be less echogenic than gas bubbles (microbubbles) because they are incompressible and do not oscillate strongly with the passing acoustic wave. However, solid and liquid particles are stable at submicron diameters and therefore can have advantageous pharmacokinetic properties. Nanoparticles can persist in circulation for hours and can be passively targeted to tumors through the enhanced permeability and retention effect, thus enhancing their reach into the tumor microenvironment.

Liquid Fluorocarbon Nanoparticles

Nanodrops are a type of liquid-liquid emulsion. The emulsion is formed by mechanical diminution of the fluorocarbon liquid into an aqueous phase. Droplet size can be controlled by sonication and extrusion techniques, as well as surfactant film curvature, to give diameters ranging between 10 and 1000 nm. The liquid fluorocarbon is dispersed in the form of small particles (nanodrops) within the aqueous phase. A surfactant layer on the fluorocarbon surface helps stabilize the tiny droplets from aggregating, coalescing, or coarsening. The surfactant layer also serves to passivate the surface from immunogenic and thrombogenic effects and provides a platform on which to attach targeting ligands and molecular contrast agents for other imaging modalities, such as magnetic resonance imaging (MRI). The fluorocarbon core can serve as a reservoir for hydrophobic drugs.

Several different perfluorocarbon emulsions have been described as echo-contrast agents. The liquid fluorocarbon phase is often highly hydrophobic, making the particles stable against dissolution. Surface tension at the fluid-fluid interface drives the particle to adopt a spherical shape and limits its deformability. Thus, from a fluid mechanics point of view, the liquid droplets act very much like solid spheres.

In general, liquid fluorocarbon nanoparticles scatter energy according to typical Rayleigh scattering theory.[1] For liquid or solid particles, the incompressibility of the interior phase prevents significant oscillation in the ultrasound field. While individual fluorocarbon nanoparticles in suspension are poorly reflecting, their aggregates can be echogenic.[2] Nanodrops therefore are suitable for applications involving high-frequency ultrasound and abundant target epitopes (to allow high accumulation by ligand-receptor interactions), such as fibrin in thrombi.[3] The inclusion of MRI contrast agents into the fluorocarbon liquid nanoparticles has made these biocolloids useful as multimodal agents (see Chapter 29, "Multimodality Agents").[4]

Another fascinating imaging application of fluorocarbon nanoparticles has been the introduction of the "phase-shift colloid," where the liquid droplet vaporizes into a gas microbubble due to thermal activation.[5] The main benefit of such an agent is the combination of the high stability of the liquid-liquid emulsion with the high echogenicity of the gas-liquid emulsion. Problems, however, include lack of surfactant coverage after area expansion from the droplet to the bubble, leading to possible coalescence. When stabilized with a polymeric coating, fluorocarbon nanoparticles can extravasate within tumors, with activation only at the desired site.[6]

Liposomes

A liposome is a vesicle formed by a lipid bilayer membrane, enclosing an aqueous core. A cartoon of an echogenic liposome is shown in Figure 1. The interior and exterior compartments are separated by a semipermeable, hydrophobic membrane. Liposomes are fabricated by lipid self assembly and postproduction processing. They can be unilamellar or multilamellar, and their size can be controlled by sonication and extrusion to range from ~20 nm to > 10 μm diameter. Typically, large multilamellar vesicles are formed by self assembly during film hydration. High-power sonication with a cell disrupter at kHz frequencies creates localized shear stresses that break up these larger aggregates into smaller, unilamellar vesicles. Further size refinement can be achieved by forcing the liposomes through well-defined, microscale pores (extrusion). The virtually unlimited library of available lipids yields a vast array of physicochemical properties, ranging from permeability to charge density to expression of specific ligands. The interior space can be loaded with other imaging agents (eg, fluorescent compounds) or with hydrophilic drugs for therapeutic applications.

Echogenic liposome formulations have been described.[7,8] The mechanism of echo contrast appears to be the backscatter from entrapped pockets of air within the liposomes that form during rehydration of the freeze-dried liposomes.[9] Similar to nanodrops, liposomes could be used as molecular imaging contrast agents in applications involving high-frequency ultrasound (eg, intravascular) and copious target epitopes.

The advantages of liposomes as ultrasound agents include their favorable pharmacokinetics, with a circulation half-life that can be extended over several days (Figure 2A).[10] In addition, when the particle diameter is

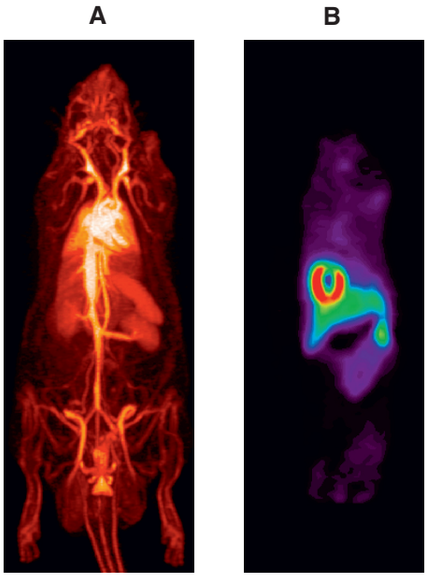

Figure 2. Positron emission tomography images obtained over 90 min after injection of liposomes. *A*, ^{18}F-fluorodipalmitin image of liposomes stably circulating. Reproduced with permission from Marik J *et al.*[10] *B*, ^{18}F-fluorodipalmitin image of liposomes coated with the lipo-PEG-peptide CRPPR adherent to the heart muscle. Reproduced with permission from Zhang H *et al.*[11]

small (~100 nm or less), vascular targeting can be very rapid and efficient[11] (Figure 2B).

Other Particles

Other echogenic particles have been found to produce detectable backscatter for ultrasound imaging. These include amorphous solid particles that contain gas pockets in their pores and fissures (so called "bubbicles").[12] Similar to liposomes, gas pockets formed during rehydration may account for the detectable acoustic backscatter. The formation of these gas pockets depends strongly on the size and shape of surface features on the particle. Such particles can be submicrometer in size, and the gas pockets can be highly stable due to pinning of the interfacial contact lines within the solid crevices. Silica nanoparticles have also been tested as ultrasound contrast agents.[13]

THE ECHOGENIC MICROBUBBLE

The microbubble is an ideal ultrasound contrast agent because it is extremely echogenic, as well as being biocompatible, multifunctional, and economical. Microbubbles are gas spheres between 0.1 and 10 μm in diameter and are much smaller than the wavelength of diagnostic ultrasound, which is typically 100 to 1000 μm. The gas core has a low density and is highly compressible, allowing it to shrink and expand with the passage of an acoustic wave. The microbubble increases and decreases in diameter at a rapid velocity giving rise to a strong and unique echo (Figure 3). It is a fortuitous coincidence that the natural reaction time of a microbubble to a rapid pressure variation is on the order of microseconds. Thus, microbubbles resonate at frequencies typically used in ultrasound imaging, and resonance can be exploited to generate a very strong echo. Due to this high degree of backscatter in comparison to plasma and blood cells, a clinical ultrasound system is capable of detecting the signature from a single microbubble—a volume on the order of a femtoliter.

Since microbubbles are too small to be resolved by current ultrasound instruments, microbubble imaging techniques are designed to differentiate their echoes from those arising from tissue based on changes in the echo spectrum and the response to changes in the amplitude or frequency of the wave. This provides an opportunity to detect a single microbubble adherent to a vascular target within the space of a single voxel and to distinguish the microbubble from the surrounding tissue.

When a dilute microbubble suspension is driven by a harmonic pulse produced by a transducer element with a low peak negative ultrasound pressure (PNP), microbubble oscillation can be nearly sinusoidal with an amplitude and shape which is a linear multiple of the transmitted wave (Figure 4A, B). Increasing the pressure of the driving pulse or introducing a nearby boundary alters the oscillatory dynamics (Figure 4C, D). With a higher ultrasonic driving pressure, the rate of collapse is very rapid—faster than the rate of expansion—with liquid inertia acting on the gas bubble to increase the rate of collapse. The nonlinear dynamics and asymmetrical profile result in echoes that contain harmonic multiples of the transmitted pulse. While tissue can also produce echoes that are rich in harmonic frequencies, substantial differences in the pressure and frequencies associated with harmonic spectra allow microbubble and tissue echoes to be differentiated. The advent of nonlinear imaging techniques has brought microbubbles to the forefront of ultrasound imaging agents.

Pulsing schemes that exploit these nonlinear features involve trains of transmitted pulses with the amplitude scaled or the phase of the pulse changed between pulses. By summing the returned echoes in a strategic manner, tissue echoes are cancelled and microbubble echoes sum coherently (Figures 5 and 6A, B); here, the CPS™ strategy of Siemens Medical Solutions is described. By imaging the intensity of the microbubble echoes, the relative vascular density within various regions can be compared.

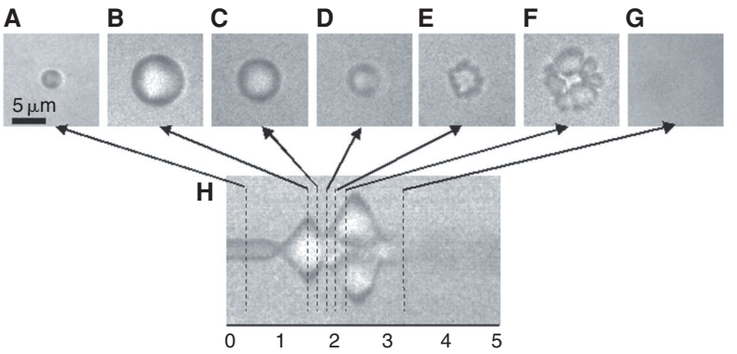

Figure 3. Two-dimensional optical frame images (A)–(G) and streak image (H) showing oscillation and fragmentation of a lipid-shelled microbubble, where fragmentation occurs during compression. Bubble has an initial radius of 1.5 μm, as shown in (A), expanding and contracting in the subsequent images. The streak image in (H), shows the diameter of the bubble as a function of time, and dashed lines indicate the times at which the two-dimensional images were acquired relative to the streak image. Reproduced with permission from Chomas JE *et al.*[81]

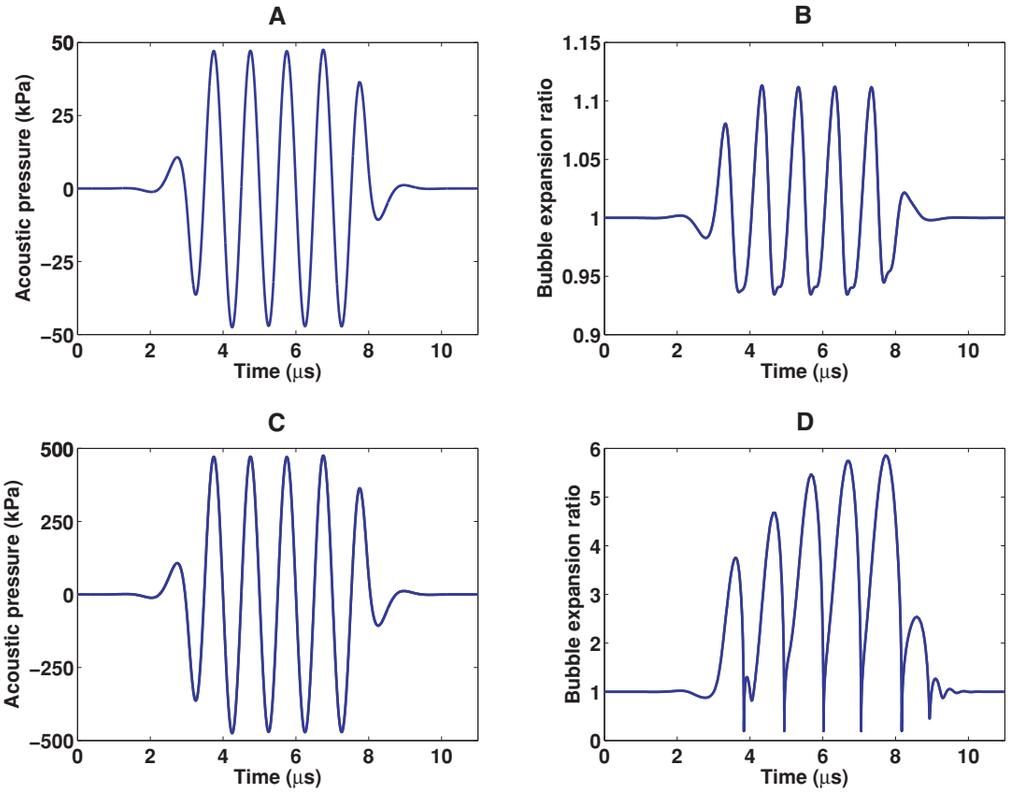

Figure 4. Effect of pulse driving pressure on bubble radial oscillations. A 1.5 radius bubble oscillates under insonation of a 5-cycle pulse with a center frequency of 1 MHz. *A*, and *B*, peak negative pressure (PNP) = 50 kPa; *C*, and *D,* PNP = 500 kPa, with driving pressure shown in (A), (C) and expansion ratio in (B), (D).

In addition, a high ultrasound pressure will result in the fragmentation of microbubbles (Figure 6D, E). Following their fragmentation and disappearance, the refill of new agents into the vasculature can be detected and the rate quantified (Figure 6C, F), allowing real-time images of vascular function (Figure 6B, C).

DOSE AND PHARMACOLOGY OF MICROBUBBLES

Little is currently known about the proper dose and pharmacology of targeted microbubbles for use in molecular imaging. Such data has been published for blood pool

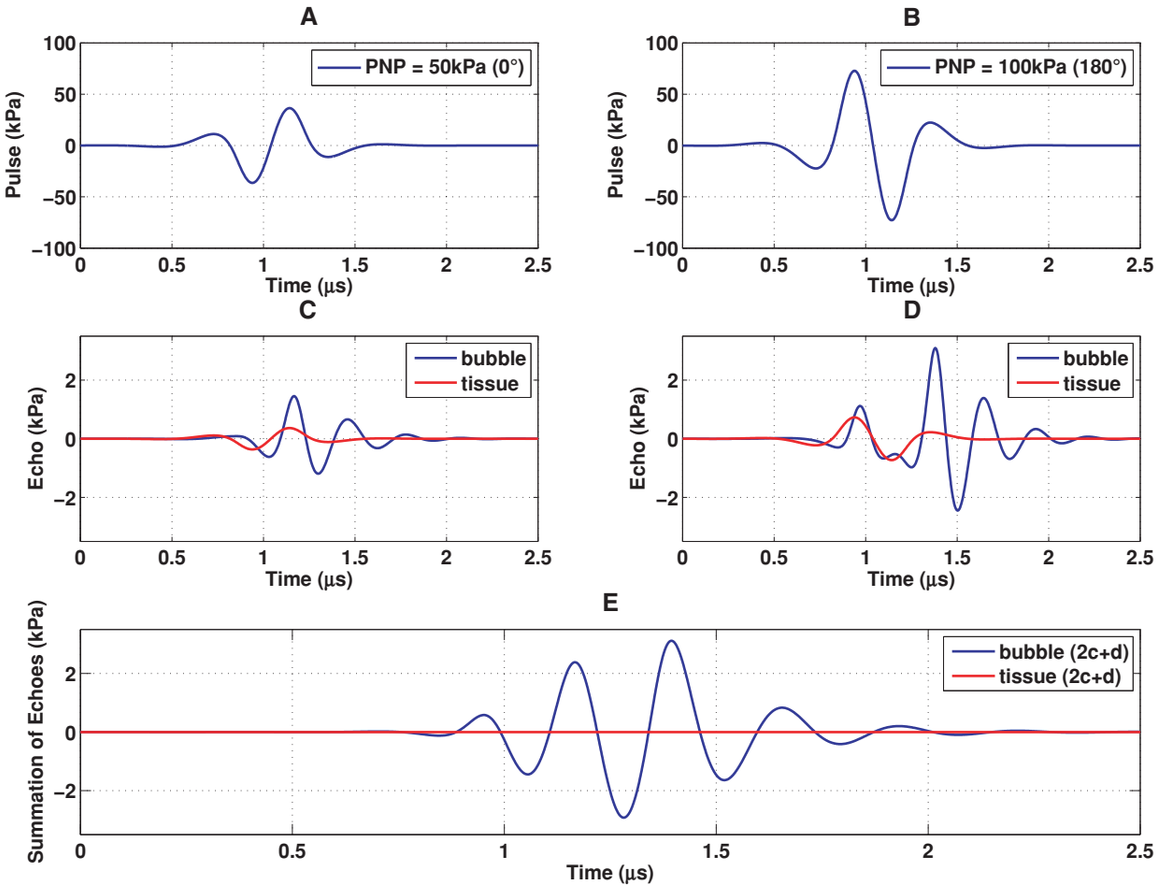

Figure 5. Illustration of a contrast pulse sequence (CPS) imaging strategy, where three scaled pulses are transmitted with scaling factors of 1/2, –1, 1/2 and the three returned echoes are summed. Shown is a one-cycle transmitted pulse with a center frequency of 2.4 MHz, with PNP of (A) 50 kPa and (B) 100 kPa. The corresponding echoes from a 1-micron bubble and tissue are shown in (C) and (D), where the echoes from the first and third pulses in the sequence would be expected to be similar. *E*, Summation of 2 times echo in (C) plus echo in (D). The linear echoes from tissue are cancelled while nonlinear echoes from the bubble are acquired.

contrast agents approved for echocardiography, which is described below. However, targeted microbubbles have inherently different and unique surface chemistries (Figure 7A), owing to the targeting ligands, and therefore could exhibit distinctly different pharmacokinetics. Clearly, immunogenicity of the targeted microbubbles is a key concern.

The first Food and Drug Administration (FDA)-approved microbubble contrast agent for ultrasound imaging was Albunex® (GE Healthcare Systems), which has an air core encased by an albumin shell. So-called "second-generation" microbubble contrast agents were developed shortly thereafter to contain a fluorinated gas core, which significantly increased the stability in blood as described below. Optison™ (GE Healthcare Systems) is now an FDA-approved protein-shelled microbubble contrast agent, which contains a perfluoropropane (perflutren) gas core. The indicated use is in patients with suboptimal echocardiograms to opacify the left ventricle and to improve the delineation of the left ventricular endocardial borders. Dose information for Optison and other commercial agents is given in Table 1. Following injection, most of the gas is eliminated through the lungs in the first 10 minutes, with a recovery of 96 ± 23% (mean ± SD) and a pulmonary elimination peak at 30 to 40 seconds after administration and half-life of 1.3 ± 0.69 minutes. The protein shell is believed to be handled through normal metabolic routes for human serum albumin, which includes degradation by proteases in the liver. Definity® (Lantheus Medical Imaging) was the first phospholipid-shelled, fluorocarbon-gas filled agent to receive FDA approval. Gas elimination routes and shell metabolism likely are similar to Optison.

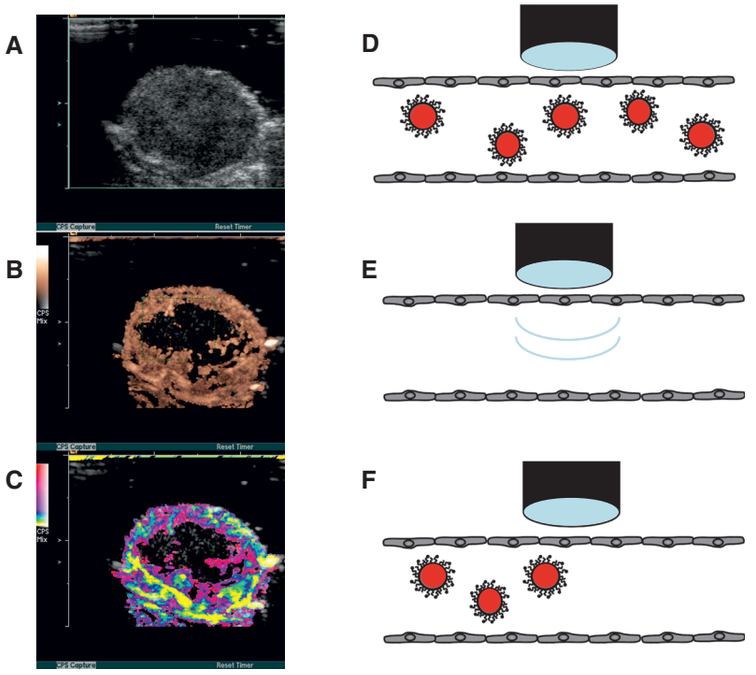

Figure 6. Ultrasound images and acquisition strategy for the estimation of flow rate. *A*, B-mode image of a Met-1 tumor[158] in a mouse model. *B*, Corresponding image of microbubble density (color) overlaid on the B-mode image, where multipulse (CPS) imaging was used to detect the presence of the microbubbles. *C*, Corresponding flow rate image, with color indicating the time required for microbubbles to refill a voxel. *D–F*, Methodology for the acquisition of replenishment images. *D*, Microbubbles fill a region. *E*, A destruction pulse removes all circulating agents. *F*, Microbubbles refill the region and their signal is detected.

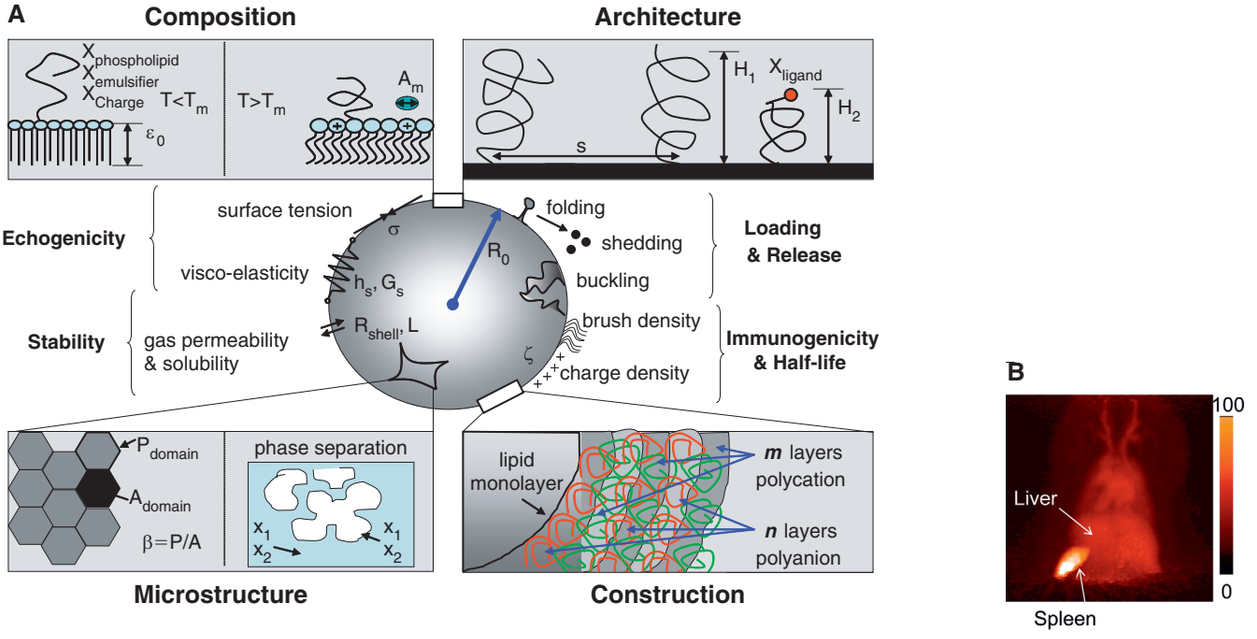

Figure 7. Microbubble basics: Design and pharmacokinetics. *A*, Schematic representation showing principles of the rational design of a microbubble for molecular imaging. The composition, architecture, microstructure, and construction can all be engineered to change the physicochemical properties, as discussed in the text. The physicochemical properties, in turn, control the performance, such as echogenicity, stability, and immunogenicity. *B*, 90-minute maximum intensity projection positron emission tomography (PET) ^{18}F-fluorodipalmitin image of microbubble pharmacokinetics, where the microbubbles circulate for a short interval and then accumulate in the liver and spleen.

Table 1. REPORTED DOSES FOR COMMERCIALLY AVAILABLE MICROBUBBLE CONTRAST AGENTS

Formulation	Shell/Gas	Concentration (mL^{-1})	Mean Diameter (μm)	Recommended Dose (μL/kg)	Maximum Dose (mL)
Optison	Albumin/C_3F_8	$5.0–8.0 \times 10^8$	3.0–4.5	6*	10.0†
Definity	Lipid/C_3F_8	1.2×10^{10}	1.1–3.3	10*	1.3‡
Imagent	Lipid/C_6F_{14}	$5.9–13.7 \times 10^8$	6§	6*	Single dose only

*Bolus intravenous injection into peripheral vein.

†Bolus administrations within 10 min; maximum of 8.7 mL in any one patient study.

‡Infusion: diluted in 50 mL saline and administered up to 10.0 mL/min.

§Based on volume-weight, all other mean diameters expressed as number-weight.

Note that commercially available ultrasound contrast agents are polydisperse in size, thereby making ambiguous the classification by average diameter.

Microbubbles exhibit similar mechanical properties to erythrocytes as they circulate in the blood. They have a similar size and deformability and therefore tend to migrate with red blood cells to the vessel center in parabolic, steady flow.[14] Intravital microscopy studies have confirmed that microbubbles have similar velocities to red blood cells in arterioles, venules, and capillaries.[15–17] When they become lodged in a blood vessel, they simply dissolve, deform, and become dislodged without significant vascular effects, as is observed for normal leukocyte plugging.[17,18] Safety issues regarding ultrasound contrast agents are covered at the end of this chapter. Positron emission tomography (PET) imaging of a lipid-shelled agent demonstrated that circulation was short lived and accumulation in the liver and spleen is significant, with some variation according to the model system. PET imaging of microbubble biodistribution in a rat model is shown in Figure 7B,[19] and that of a mouse model is shown by Willmann and colleagues.[20]

Despite the biocompatibility of the materials used to fabricate microbubbles (eg, proteins, lipids, and biopolymers), microbubbles tend to be decorated with immunological markers present in the blood (ie, they become opsonized) and eliminated from circulation via the reticuloendothelial system (RES). Early studies with protein-coated microbubbles showed clearance by macrophages.[21,22] Consistent with the location of macrophages in different animal models, roughly 60% of radio-labeled Albunex was found to accumulate in the liver (Kupffer cells) of rats, whereas 90% accumulated in the lungs of pigs.[22] Phagocytic accumulation can provide a means of imaging physiologic processes related to immune function *in vivo*.[23] Opsonization and leukocyte attachment of microbubbles can also be used to image vascular events, such as ischemia/reperfusion[24] and atherosclerosis.[25,26]

Lipid-coated microbubbles can be engineered to limit clearance by phagocytosis. For example, SonoVue® (Bracco Diagnostics Inc.) was found to evade liver clearance,[27] whereas Sonazoid™ (GE Healthcare) was found to be exclusively phagocytosed by Kupffer cells.[28] As with liposomes, the mechanism of clearance depends on the surface chemistry (as well as diameter). For example, anionic microbubbles exhibit different pharmacology than cationic microbubbles.[24,29]

PHYSICOCHEMICAL PROPERTIES OF MICROBUBBLES

Rational design principles can be applied to the formulation of superior molecular imaging contrast agents. Figure 7A shows a schematic diagram detailing some of the means by which a microbubble may be engineered. The physicochemical properties can be controlled through concepts in biocolloid engineering design, including composition, microstructure, architecture, and construction. In turn, these physicochemical properties affect the final performance of the microbubble in a molecular imaging study.

Microbubble Fabrication

Various methods have been used to fabricate microbubbles for ultrasound imaging. The most popular method has been emulsification by entrainment of a gaseous hood into the aqueous phase by mechanical agitation of the gas-liquid interface. Methods of diminution include shaking (amalgamation) and sonication. These techniques rely on stochastic events that produce a polydispersed size distribution, generally ranging between submicrometer to tens of micrometers in diameter. Size fractionation techniques can be employed, which are based on buoyancy.[30] Newer techniques have been developed to produce monodisperse microbubbles. These microfluidic methods include flow focusing,[31,32] T-junctions,[33] jetting,[34] and electrohydrodynamic atomization.[35]

Diminution techniques provide rapid and cost-effective microbubble generation that can be done at the bedside. Microfluidic technologies will need to show similar robustness and ease of preparation in generating a sufficient microbubble dose. However, the potential gains in control over the microbubble surface chemistry and size could significantly enhance quantification in molecular imaging studies.

Several methods have been described to encapsulate gas in a polymer shell. Dispersion and ionic gelation have been used to create alignate-shelled microbubbles.[36] Organic solvents have been used to dissolve and disperse the polymer, which is then resuspended to form hollow polymer capsules.[37–39] A technique involving partial filming of surfactant-coated microbubbles with nanoparticles was recently described by Schmidt and Roessling.[40] Polymerization at the air-liquid interface during agitation of an acidic medium was used by Cavalieri and colleagues.[41] Each of these methods has produced microbubbles with enhanced stability. However, chain entanglement and covalent bonds inherent in the polymer shells severely dampen the oscillation of the gas core,[42,43] thus reducing echogenicity prior to shell rupture.

Microbubble Stability

A clean microbubble is inherently unstable owing to surface tension (σ) of the gas-liquid interface (~72 mN/m for an air-water interface). Any gas-liquid or liquid-liquid interface will, by definition, exhibit a surface tension owing to disruption of cohesive intermolecular forces. A force balance over the curved surface reveals a net pressure that is greater on the concave side (ie, inside the microbubble). The overpressure inside the microbubble (ΔP) was given by Young and Laplace[44]:

$$\Delta P = P_b - P_a = \frac{2\sigma}{R}, \qquad (1)$$

where P_b is the total pressure inside the bubble, P_a is the ambient pressure, and R is the bubble radius. For a microbubble, the overpressure is on the order of an atmosphere. According to Henry's Law, the overpressure increases the local solubility of the gas at the microbubble surface, thus creating a chemical potential gradient over which gas diffuses into the surroundings. Thus, surface tension drives the dissolution of the microbubble.

Epstein and Plesset derived an ordinary differential equation for the transport of gaseous species into the surrounding medium.[45,46] The model was formulated by taking a mass balance over the microbubble and coupling it to the diffusion equation to arrive at the following expression for the microbubble radius (R) as a function of time (t):

$$-\frac{dR}{dt} = \frac{LD_w}{R}\left(\frac{1+\frac{2\sigma_{shell}}{P_a R}-f}{1+\frac{4\sigma_{shell}}{3P_a R}}\right), \qquad (2)$$

where L is Ostwald's coefficient, D_w is the gas diffusivity in water, R_{shell} is the resistance of the shell to gas permeation in Eq. (3), σ_{shell} is the surface tension of the shell, and f is the ratio of the gas concentration in the bulk medium versus that at saturation. This model neglects the time to develop the concentration boundary layer and assumes a perfectly spherical geometry for a microbubble dissolving in an isotropic medium.

The Epstein-Plesset equation predicts that a free air microbubble will completely dissolve within a second in saturated water (Figure 8). One approach to increase stability has been to use hydrophobic gases, such as perfluorocarbons, which have water permeation resistances ($L^{-1}D_w^{-1}$) that are several orders of magnitude higher than air.[47,48] The water permeation resistance of n-C_4F_{10}, for example, is over 100 fold greater than that of air. The molecular weight, M, and other properties of relevant gases in saline are summarized in Table 2. The molecular weight and solubility of air are approximated by that of N_2, the principal component of air, and the molecular weight and solubility of N_2 are shown in parentheses. The diffusivity values of n-C_3F_8 and n-C_4F_{10} are obtained

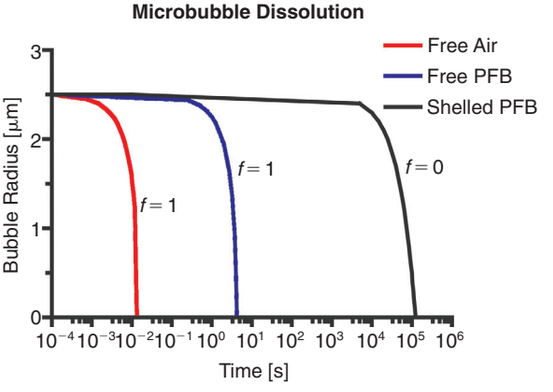

Figure 8. Radius versus time predicted for microbubbles of different composition dissolving in a static, isotropic medium. Changing the gas content from air [free air] to perfluorobutane for an unshelled microbubble [free PFB] increases the lifetime in a saturated medium, but the gas still dissolves within a minute due to surface tension. Adding a solid phospholipid shell [shelled PFB] significantly enhances the predicted lifetime, even in a completely degassed medium.

Table 2. GAS PARAMETERS USED IN THE MODELING OF MICROBUBBLE DISSOLUTION TIME

Gas	Molecular Weight, M (g/mol)	Solubility, $L \times 10^3$ (cm^3/cm^3)	Diffusivity, $D_w \times 10^6$ (cm^2/s)
Air (N_2)	(28)	(15)	20
n-C_3F_8	188	4.6	7.7
n-C_4F_{10}	238	0.51	6.9

from the Stokes-Einstein approximation, which is based on the assumption that the molecular weight is proportional to R_m^2, where R_m is the molecular radius. The solubility of n-C_3F_8 and n-C_4F_{10} in water at 20°C is more than five times larger than that in water at body temperature (37°C).[49] Although the use of n-C_4F_{10} or n-C_3F_8 can increase microbubble lifetime by an order of magnitude or more (see Figure 8), the surface tension effect drives complete microbubble dissolution within a minute, which is far too short for a molecular imaging study.

Encapsulation is therefore required to stabilize the microbubble. For appropriate stability on the shelf and *in vivo*, the microbubble shell must both eliminate surface tension and impart a significant permeation resistance. Interestingly, this can be achieved with surfactants, such as lipids below their main phase transition temperature, due to jamming of the molecules into a kinetically trapped configuration that is disordered but has solid-like character, such as high viscosity.[50,51] Removing the overpressure eliminates the driving force for dissolution in saturated media. This allows long-term storage of microbubbles, which are stable for months in a sealed vial. In addition to eliminating surface tension, the shell may contribute a resistance to gas leaving the core, as modeled by Borden and Longo[52]:

$$-\frac{dR}{dt} = \frac{L}{\frac{R}{D_w} + R_{shell}}(1-f). \qquad (3)$$

Gas permeation through the shell and diffusion in the surrounding medium are modeled here as resistances in series, analogous to electrical circuits. The shell resistance is a function of the permeating gas species and the shell composition. In convective flow, where the diffusive boundary layer becomes thin, the shell resistance becomes the dominant term.

Shell Materials

Early ultrasound contrast agents were coated with an adsorbed layer of albumin protein.[53] The albumin-coated microbubbles Albunex® and Optison™ (GE Healthcare) were the first commercially available, FDA-approved contrast agents. More recently, protein-shelled microbubbles have been functionalized to carry targeting ligands[54] and therapeutic payloads.[55,56] Albumin shells tend to be rigid and less stable to ultrasound,[57] however, and introduce the typical immunogenicity issues associated with animal-derived materials.

Phospholipid shells are most commonly used for ultrasound molecular imaging. Several phospholipid-based ultrasound contrast agents are commercially available worldwide. Lipid-stabilized microbubbles are easy to manufacture, biocompatible, and echogenic. Once a gas particle is entrained in a suspension of lipid vesicles and micelles, the hydrophobic effect drives adsorption and orientation of the lipid molecules at the gas-liquid interface to minimize surface tension. The lipid shell has a similar structure to a Langmuir monolayer at high compression, with lipid head groups oriented outward, except that it is completely self enclosed in a spherical geometry. A broad library of different lipids is available to provide stability and functionality. Most formulations for targeted microbubbles consist of three components: a matrix lipid, an emulsifying lipid, and a targeting lipid. The matrix lipid stabilizes the shell by providing cohesion and is often chosen to be below the main phase transition temperature. The emulsifying lipid usually contains a polymeric group, such as polyethylene glycol (PEG), that aids in lipid adsorption and assembly.[58] The brush also inhibits coalescence and passivates the surface. The brush is often formed by PEG 2000 to 5000 Da; shorter PEGs (eg, 1000 Da) are unable to stabilize the microbubble. Up to 20 mol% PEGylated lipid can be incorporated.[51] On the targeting lipid, a polymer spacer is necessary to extend the ligand past the brush.[59]

Lipid composition can have a dramatic effect on microbubble properties. Longer chains provide more cohesion through enhanced van der Waals and hydrophobic interactions, which increase the shear viscosity[60] and decrease the gas permeability.[61] Longer chains also change the mechanism and kinetics of lipid collapse and shedding from vesiculation to fracture and folding.[62] This is evidenced by morphological changes in the microbubble during static dissolution[52] and in the destruction kinetics during acoustic pulsing.[63]

Surface Microstructure

The polycrystalline structure of the lipid microbubble shell was initially shown in pioneering work by Kim and colleagues.[60] Microscopy and spectroscopy evidences indicate that the shell consists of multiple phases, often exhibiting the characteristics of an ordered phase dispersed into a disordered phase.[51,64] The ordered phase tends to be populated with the matrix lipid, whereas the disordered phase tends to be enriched with the emulsifier.

Microstructure depends on both composition and processing conditions. Increasing PEG lipid concentration in the shell leads to an increase in the area fraction of the disordered phase.[51] Heating and cooling changes the morphology of the ordered phase.[51,60,64] The ordered phase can be melted by heating above the main phase transition temperature of the matrix lipid. Cooling through the transition at different rates leads to differences in domain density, shape, and size. For example, slow annealing can yield very large domains on the shell. The domains are not rigid plates; they can bend to accommodate the spherical surface.

Microstructure affects many of the same physicochemical properties as composition. Increasing the defect density produces similar results to using shorter chain lipids. The gas permeability increases[61,65] and the surface shear viscosity decreases.[60]

Surface Architecture and Ligand Chemistry

Microbubble stability is enhanced by the incorporation of a brush layer of PEGylated lipids, with concentrations of five to nine molar percent typically reported. Ligands are incorporated on the distal end of a polymer, where the polymer length can be chosen to extend beyond the brush layer to efficiently bind to their target. Architecture refers to the internal structure of the brush layer on the microbubble shell. Architecture therefore depends on both composition and microstructure (eg, the local composition and dimensions of the ordered and disordered phases). Bimodal brushes can be used. A longer spacer arm than the surrounding brush can be used to increase the ligand availability and therefore adhesion strength.[59] Alternatively, a shorter spacer arm can be used to decrease ligand availability, and therefore immunogenicity.[66,67]

The architecture of the targeting ligand depends on details of the ligand molecule and the linking chemistry. Small ligands (order 100 Da) attached to the distal end of the PEG chain will exhibit dynamics governed by the thermal motion of the polymer spacer.[68] Larger ligands (order 1000 Da), however, will significantly change polymer dynamics.[69]

Small molecule ligands can be directly attached to lipids, and the ligand-lipid conjugate is then purified prior to the incorporation in microbubbles. The methods for lipo-PEG peptide synthesis have been proposed for many years, and the details of such strategies are recently described.[11] Peptides can be synthesized manually by standard fluorenylmethoxycarbonyl (FMOC) chemistry protocols on solid phase.[70] PEG is coupled onto a peptidyl resin, and Fmoc-Lys(Fmoc)-OH and stearic acid are coupled in sequence. Lipo-PEG peptides are cleaved from the resin and purified with HPLC.

Large proteins (including antibodies) are often attached through covalent or noncovalent chemistry after the contrast agent is formed due to the harsh conditions that accompany microbubble creation. The relatively large diameter of a microbubble necessitates the use of a large number of ligands (100,000 per microbubble) to insure adequate coverage. Biotin-streptavidin approaches, in which biotin is attached to the lipid or PEG molecule, have been used most commonly[71,72] due to their simplicity. A common ligand linkage motif is biotin-avidin-biotin. Avidin contains multiple binding pockets and therefore can bind to multiple underlying biotinylated lipids. The avidin molecule has a mass of ~60 kDa and is several times larger than the underlying PEG. Furthermore, antibody molecules often have a mass of ~120 kDa. Thus, the architecture can be viewed as a scaffolding structured with a thin polymer cushion and bulky protein outer layer. To use avidin-biotin linkage, an excess of streptavidin is incubated with the microbubbles, followed by centrifugation to remove excess streptavidin. The biotintylated ligand is then added in a final step. The disadvantage of this approach is the immunogenicity of the resulting surface, rendering this approach to be inappropriate for translational studies. A protein-bearing surface, such as one with avidin and antibody, will likely have exposed nucleophilic groups, such as hydroxyls and amines, that can bind to the unstable thioester bond on the complement protein C3b. Binding of C3b to the surface of the microbubble not only changes the ligand binding properties but also marks the microbubble for clearance by the RES and proceeds with activation of the complement system and the inflammatory response. Complement activation is of course undesired for molecular imaging, which is primarily used for diagnostic purposes of the unaltered physiology. Thus, it is important to shield the ligand by covering it with a methoxy-terminated PEG overbrush. The ligand can be revealed by ultrasound oscillation and radiation force, as discussed later.

Covalent attachment strategies have also been implemented. The advantages and disadvantages of carboxylic acid-amine approaches, in which a carboxylated

lipid derivative is incorporated into the microbubble shell and reacts with an amine on the ligand, were described in detail by Klibanov.[71] Potential side products of this reaction include the formation of N-acylisourea, which bind to the microbubble shell.[71] A more efficient strategy for postlabeling with antibodies has been developed using a maleimide-thiol approach, in which a maleimide-PEG-lipid is incorporated in the monolayer shell and reacts with a thiol-containing targeting ligand.[71,72] Maleimide reactive groups are more stable in aqueous buffers than an NHS buffer, side reactions are reduced, and a greater percentage of the ligand binds to the target site.

Surface Construction

Construction refers to the addition of shell components after formation and stabilization of the initial lipid-coated microbubble. Therefore, construction adds another layer of architectural complexity. In addition to avidin-biotin linkage chemistry, other materials can be constructed onto the lipid monolayer shell. For example, clustered polymeric forms of ligands have been used to enhance adhesion in high-shear flow.[73]

Another means of construction involves the deposition of oppositely-charged polyelectrolytes as in layer-by-layer assembly. Such layering can significantly change the properties of the shell. Multilayer shells were shown to enhance the stability of the gas core against dissolution.[74] Further, multilayer shells were shown to increase the number of plasmid DNA molecules that could be loaded per microbubble.[75] Interestingly, multilayers were shown to slightly dampen the oscillation of the microbubble (compared to just a lipid-coated agent of similar gas-core diameter) although the damping effect disappeared after the first few cycles.[75]

BIOMEDICAL PERFORMANCE OF MICROBUBBLES

Insonified Microbubbles

Sophisticated experimental systems, which incorporate microscopes, custom strobe lights or lasers and high frame-rate cameras, have been developed to measure microbubble dynamics during oscillation at megaHertz frequencies.[57,76–80] High spatial and temporal resolution is necessary due to the small size of the microbubble and the rapid oscillations they incur during vibration in the ultrasound field. Optical observation provides information on the dynamic motion of ultrasound microbubbles during insonation that is unavailable with traditional methods of analyzing the received echoes from contrast agents or modeling of bubble motion. Diffraction effects associated with the gas-liquid interface are used to characterize the dynamics of the gas core; fluorescent probes are inserted within the lipid shell to follow translation of the shell material and its association with the gas bubble over time. Very high-speed cameras with a shutter duration of picoseconds to nanoseconds are used to capture two-dimensional images of the microbubble oscillation; typically, the number of recorded images is limited and the time duration available for recording is less than 1 ms.[79,81] In addition, "streak" cameras continuously record the oscillation of a single line across the microbubble diameter although again over a time window limited to a small fraction of a second.[81] An alternative approach has been to use a very bright strobe with a short duration, such as that produced by a high duty cycle laser, to illuminate the sample while recording observations with a slower camera.[57,78] This approach has proven to be successful in imaging the oscillation of microbubbles within blood vessels and in recording events that require large numbers of pulses within a single position.

Gas Dissolution During and After Insonation

Dissolution kinetics change when the shell properties are altered during insonation, as shown through microscopy. Prior to insonation, dissolution is not apparent on typical optical timescales of observation (seconds). One example of the altered dynamics is shown in Figure 9A, where a single one-cycle ultrasound pulse with a peak negative pressure of 240 kPa and center frequency of 2.25 MHz occurred at the time shown by the arrow. The lipid-shelled agent decreases in diameter at the time of the pulse (the time interval from 90–120 ms); however, the diameter remains constant after the completion of the pulse (dashed lines) for the remaining 5 s of observation. In this case, the lipid-shelled microbubble contains C_4F_{10}, where unencapsulated gas bubbles of C_4F_{10} are predicted to dissolve into the surrounding liquid within 5 s. By comparison, the diameter of the albumin-shelled agents continues to decrease after the end of the ultrasound pulse (solid lines). Further, when a train of ultrasound pulses (peak negative pressure of 240 kPa and center frequency of 2.25 MHz) is directed to lipid-shelled microbubbles (Figure 9B), a decrease in diameter of ~0.11 μm is observed with each pulse, with the diameter again remaining constant between pulses. Thus, the lipid-shelled agents show a small, rapid decrease in diameter

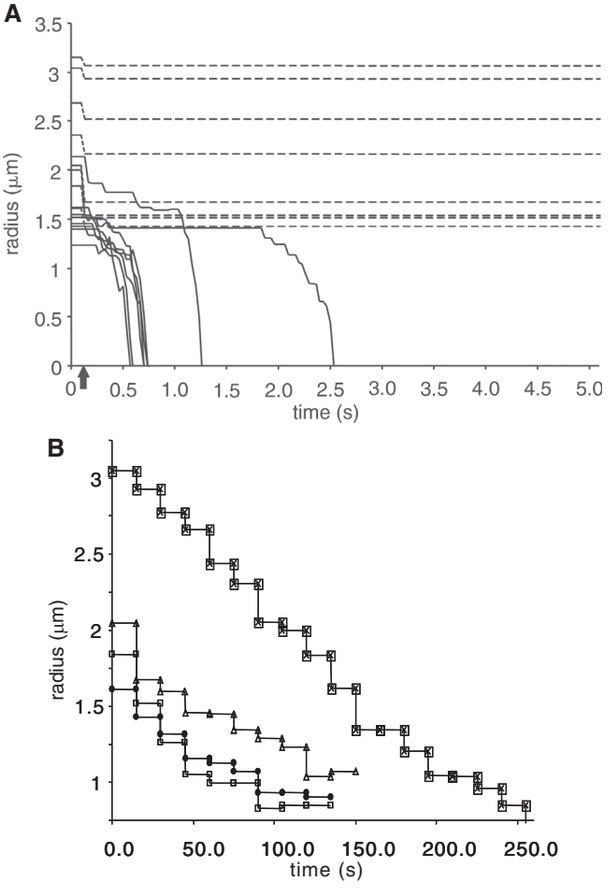

Figure 9. Microbubble dissolution after insonation. *A*, Radius versus time obtained from 30 frames per second images of phospholipid-shelled and albumin-shelled agents (arrow indicates time of ultrasound pulse). All bubbles are insonified with a single-cycle pulse of 240 kPa transmission pressure at time = 90 ms, signified by the vertical arrow along the abscissa. Albumin-shelled agents (solid lines) decrease in radius due to static diffusion. Lipid-shelled agents (dashed lines) decrease in diameter with each pulse but remain intact between pulses. Reproduced with permission from Chomas JE *et al.*[100] *B*, Change in lipid-shelled microbubble diameter over a train of pulses, demonstrating decreased diameter with each pulse (mechanism of acoustically-driven diffusion). Each bubble is insonified by one single-cycle pulse every 15 s. No decrease in radius is observed between pulses. The decrease in radius observed immediately after insonation is due to acoustically-driven diffusion. Reproduced with permission from Chomas JE *et al.*[100]

coincident with the ultrasound pulse and then remain unchanged for an extended period that is greater than the time required for static dissolution of the remaining gas into the surrounding liquid. The magnitude of this step change per cycle is a function of the coating lipid.[63] Therefore, the concept of "shell rupture" often thought to be associated with insonation of shelled microbubbles is not an accurate description of lipid-shelled microbubble behavior. As opposed to the stability of lipid-shelled agents after insonation, albumin-shelled agents exhibit static dissolution after insonation, with a dissolution rate on the order of that predicted by equations for an unshelled gas bubble.

Theoretical Predictions of Microbubble Oscillation

The radial motion of a single ultrasound contrast agent under insonation can be captured by the Rayleigh-Plesset equation that assumes the liquid is incompressible and infinite.[82–85] To apply the Rayleigh-Plesset equation, one usually assumes that the gas in the bubble has uniform pressure and obeys the polytropic gas law, which requires that the velocity of the bubble wall is small relative to the speed of sound in the surrounding medium.[86] Under these assumptions, the equation of motion for the bubble wall has the form:

$$\ddot{R}R + \frac{3}{2}\dot{R}^2 = \frac{1}{\rho}\left[\left(p_0 + \frac{2\sigma}{R}\right)\left(\frac{R_0}{R}\right)^{3\kappa} - \frac{2\sigma}{R} - \frac{4\eta\dot{R}}{R} - p_0 - p_i(t)\right], \quad (4)$$

where R_0 is the bubble radius at equilibrium, $\dot{R}$ and $\ddot{R}$ represent, respectively, the first- and second-order time derivatives of the bubble radius R, p_0 is the hydrostatic pressure, $p_i(t)$ is the incident ultrasound pressure in the liquid at an infinite distance from the microbubble, κ is the polytropic exponent, and ρ, σ, and η are the density, surface tension, and viscosity of the bulk fluid, respectively. The bubble will behave isothermally (ie, $\kappa \approx 1$) if the thermal diffusion length in the gas is greater than the bubble radius, whereas it will behave adiabatically (ie, $\kappa \approx \gamma$, the specific heat ratio of the gas within the bubble) if the thermal diffusion length in the gas is much smaller than the bubble radius and the bubble radius is much less than the wavelength of sound in the bubble.[87] In the framework of the linearized theory, the bubble resonance frequency can be obtained by the well-known results of Minnaert[88]:

$$\omega_0 = \frac{1}{R_0}\left[\frac{3\kappa}{\rho}\left(p_0 + \frac{2\sigma}{R_0}\right) - \frac{2\sigma}{\rho R_0}\right]^{\frac{1}{2}}. \quad (5)$$

The pressure of emitted ultrasound at distance r from the bubble center is as follows:

$$p(r) = \frac{\rho R}{r}(2\dot{R}^2 + R\ddot{R}). \quad (6)$$

When the incident pressure wave is increased, the ratio of the velocity of the bubble wall to the sound speed in the liquid ($\dot{R}/c$) approaches unity, and sound radiation becomes important. A number of Rayleigh-Plesset derivatives have been proposed, particularly modifications that account for sound radiation, including the Keller equation, the Herring equation and the Gilmore equation.[89–99]

Observations of Microbubble Oscillation

Under limited conditions, oscillation is nearly symmetrical. The center frequency, pressure, and phase of the transmitted pulse alter the oscillation of lipid-shelled microbubbles.[100,101] Decreasing the center frequency and increasing the peak negative pressure act to increase the maximum expansion and the rate of microbubble collapse. When relative expansion, defined as the ratio of maximum to initial diameter, exceeds a threshold (~3), the bubble is unstable and is frequently observed to fragment into smaller daughter bubbles. These smaller gas bubbles often recombine with subsequent ultrasonic cycles, and cycles of fragmentation and fusion are observed with long transmitted pulses. The oscillation and fragmentation of a lipid-shelled microbubble are shown in Figure 3, combining a set of two-dimensional frame images of expansion and contraction with a continuous "streak" recording of a single line through the center of the microbubble. At a time near 2 μs and between images D and E, the microbubble fragments, with a set of small bubbles observed after this time point.

As a basis of comparison, BG1135 (Bracco Research S. A., Geneva, Switzerland) is a polymer-shelled, air-filled microsphere with a rigid, 100 nm thick shell. Expansion and contraction of these microbubbles is not evident until the shell ruptures (Figure 10). Upon insonation with sufficient ultrasound pressure, the microbubble suddenly ejects a gas bubble. Gas bubble extrusion, ejection, and displacement by microns are observed on a timescale of microseconds[100], still a relatively low velocity compared with the wall motion during oscillation.[81] A summary of the oscillation of lipid and polymer-shelled microbubbles is provided in Figure 11. The lipid-shelled microbubbles (see Figure 11A) insonified under the same conditions expand with relative expansion determined by their initial radius, and fragmentation depends on expansion. Polymer-shelled microbubbles (see Figure 11B) insonified at a low pressure do not expand, whereas those insonified at a higher pressure expand and fragment. We have also reported ejection of a gas bubble through a shell defect in Optison agents, which have a semirigid albumin shell.[57] We observed that the resulting gas bubble moved away from the shell (traveling several microns in milliseconds), and that the shell collapsed after the gas bubble was ejected.

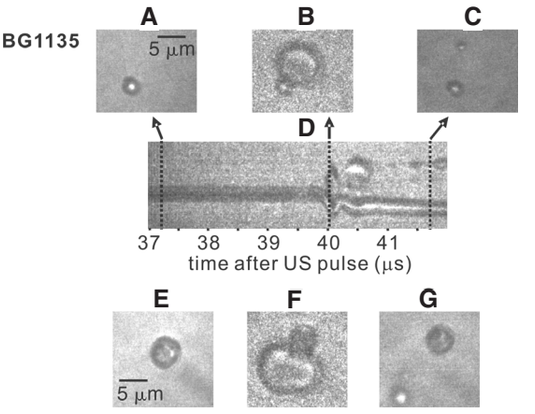

Figure 10. Oscillation and destruction of polymer-shelled agent BG1135. Still images (A)–(C) depict the agent before, during, and after exposure to a 2-cycle, 2.25 MHz, 1.4 MPa ultrasound pulse. The streak image (D) shows one line of sight through the agent versus time, with the acquisition times of the still images indicated. The agent is observed to acquire a shell defect and subsequently to eject a new fragment some distance from the original agent. Images (E)–(G) show destruction of another polymer-shelled bubble in response to a 2-cycle, 2.25 MHz, 1.2 MPa pulse. Reproduced with permission from Bloch SH *et al.*[43]

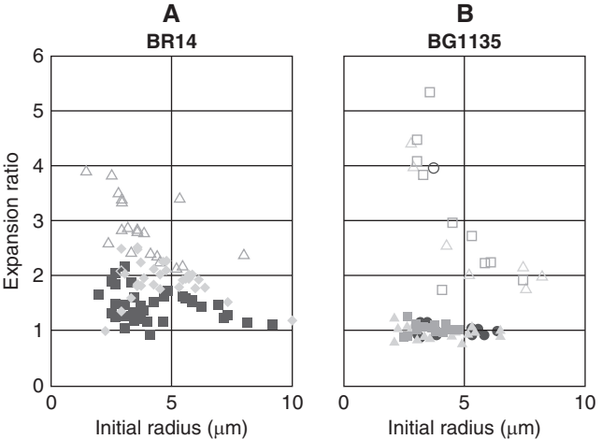

Figure 11. Expansion ratio *vs.* initial radius in response to a 2-cycle, 2.25 MHz pulse for lipid-shelled agent BR14 (A), (square, 180 kPa; diamonds, 360 kPa; triangles, 920 kPa) and polymer-shelled agent BG1135 (B), (circles, 660 kPa; triangles, 1.2 MPa; squares, 1.4 MPa). Closed symbols indicate bubbles intact after insonation; open symbols indicate fragmented bubbles. Reproduced with permission from Bloch SH *et al.*[43]

The Effect of the Microbubble Shell and Constraining Vessels

The shell changes the bubble's mechanical properties including resonance, viscous damping, and scattering properties. De Jong and colleagues[102–105] treated the bubble shell as an elastic solid layer and theoretically studied acoustic attenuation, backscatter, and nonlinear oscillation, which was validated by experimental results. Church[106] derived a Rayleigh-Plesset-like equation describing the dynamics of an encapsulated gas bubble, assuming that the coating material is a layer of incompressible solid elastic material. Hoff and colleagues[107] developed a model that included viscous and elastic properties of the shell to describe polymeric microbubble behavior. The resonance frequency of a polymeric gas bubble was described as follows:

$$\omega_0 = \frac{1}{R_0}\left[\frac{3\kappa}{\rho}\left(p_0 + \frac{2\sigma}{R_0}\right) - \frac{2\sigma}{\rho R_0} + \frac{12G\varepsilon_0}{\rho R_0}\right]^{\frac{1}{2}}, \qquad (7)$$

where G is the shear modulus of the shell and ε_0 is the initial shell thickness at equilibrium. Equation (7) shows that the resonance frequency tends to decrease as bubble size increases and to increase as the modulus of the shell rigidity increases (Figure 12A). The resonant nature of the unshelled microbubble can also be recognized by the narrow peak in the scattering cross section, which is defined as the power scattered per unit volume. The scattering cross section of a shelled microbubble is predicted to peak at a higher frequency than the unshelled microbubble; however, the peak is substantially broadened (Figure 12B). Church's studies[106] indicate that for bubbles with a diameter in the range of ultrasound contrast agents ($R_0 \leq 10$ μm), the damping effects of the bubble shell are dominated by viscous, compared with thermal mechanisms, and that the attenuation coefficient in a bubbly liquid decreases as either the rigidity or the viscosity of the bubble shell increases.

The oscillation of microbubbles in small blood vessels at target sites is of great interest for applications in molecular imaging and ultrasound-enhanced drug and gene delivery. Microbubble oscillation in small vessels is substantially different from that predicted by the Rayleigh-Plesset equation. Thus, there have been increasing efforts to model microbubble oscillation in small vessels.[108–115] The models can be summarized into two areas: linear approximation and direct numerical simulation based on the Navier-Stokes equation. Microbubble oscillation in these systems is quite complex.

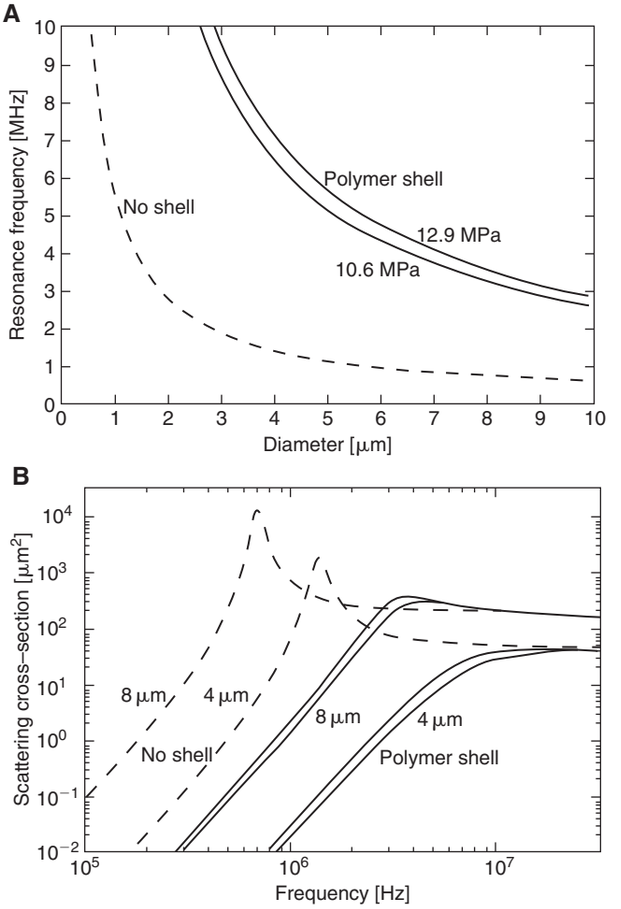

Figure 12. Changes in microbubble properties with diameter and materials. *A*, Calculated resonance frequency as function of particle diameter. The solid lines show the values found for the bubble encapsulated in a polymer shell, whereas the dashed line shows values calculated for free air bubbles. The two curves for the polymeric microbubbles correspond to the shear modulus *G* = 10.6 MPa, shear viscosity μ = 0.39 Pa·s and G = 12.9 MPa, μ = 0.49 Pa·s. Reproduced with permission from Hoff L *et al.*[107] *B*, Scattering cross section as function of frequency. Calculated for polymer-encapsulated air bubbles (solid lines) and for air bubbles without shells (dashed lines) with diameters 4 and 8 μm. The two curves for the polymeric microbubbles correspond to the shear modulus *G* = 10.6 MPa, shear viscosity μ = 0.39 Pa·s and G = 12.9 MPa, μ = 0.49 Pa·s. Reproduced with permission from Hoff L *et al.*[107]

The bubble oscillation not only depends on the shell material properties and the acoustic parameters (eg, pressure, frequency, and pulse length) but also on the size and mechanical properties of the vessel. The linear oscillation frequency of a bubble decreases within small rigid vessels[113,116] and increases within small compliant vessels.[112] In small vessels, bubble oscillation is asymmetrical, and expansion is reduced for rigid vessels. Within small compliant vessels, bubble oscillation increases the pressure across the vessel wall and therefore could enhance vascular permeability.[111] For 0.5

MPa (or larger) and 1 MHz ultrasound pulses, bubble oscillation induces a large circumferential stress within the vessel wall that may exceed the vessel strength. The induced stress within the vessel wall has a stronger dependence on insonation frequency than suggested by mechanical index ($MI = P/\sqrt{f}$).[111]

Experiments have shown results consistent with those predicted by theoretical models. Compared with bubble oscillation within infinite liquids or large vessels, bubble maximum expansion within small vessels is decreased while the lifetime is increased.[78,117] The threshold of bubble collapse has been found to depend not only on the applied pressure amplitude but also on the vessel size, with an increase for smaller silica vessels.[114] *Ex vivo* studies have shown that during insonation, small bubbles tend to fuse into larger bubbles (≥ 10 μm), and these fused bubbles can displace the vessel wall up to a few microns.[118] Vessel wall deflection increases with increasing initial bubble size and decreasing vessel diameter. Optical observation has shown that phagocytosed microbubbles experience viscous damping within the cytoplasm and yet remain acoustically active and capable of large volumetric oscillations during an acoustic pulse.[118] Phagocytosed microbubbles produce an echo with a higher mean frequency than free microbubbles in response to a rarefaction-first, single-cycle pulse.[118]

DELINEATING ADHERENT MICROBUBBLES

Microbubbles adherent to a vessel surface have been shown to oscillate asymmetrically and with a lower volumetric increase and decrease compared with free microbubbles.[119] Still, greater echo harmonic energy is produced by adherent microbubbles than surrounding tissue. Adherent and free microbubbles can be distinguished based on their pulse-to-pulse motion, since adherent microbubbles move at a velocity that is comparable to tissue. Therefore, signal processing methods can be developed to distinguish between bound and free microbubbles based on the individual pulse echo and the echoes obtained over a pulse train.[119]

EXAMPLES OF MOLECULAR TARGETING

Microbubbles are targeted effectively to vascular receptors accessible to the luminal space, including those associated with inflammation, thrombus, and angiogenesis. Proof of concept was demonstrated by Klibanov and colleagues,[73] where targeted microbubbles incorporating a biotinylated shell component (0.15–7.5 mol%) adhered to avidin-coated petri dishes, remaining adherent to the dish under tangential flow rates up to 0.6 m/s. Flowing microbubbles and their cargo can adhere to the surface of a vessel with applied ultrasound radiation pressure.[119,120] We briefly describe examples of targeted microbubble imaging here; further examples are provided in Chapter 40, "Protein Engineering for Molecular Imaging".

Inflammation

Changes in endothelial receptors occur rapidly after the onset of an inflammatory stimulus, and these receptors have been effectively targeted with microbubble contrast agents. VCAM-1 and ICAM-1 have been shown to be upregulated in sites of atherosclerotic lesion formation.[121] P-selectin is available on the endothelial surface shortly after ischemic events.[122] Leukocytes are recruited to the site of inflammation and also serve as early inflammatory targets.

Nonspecific interaction between microbubbles and leukocytes was exploited in early studies of targeted imaging of inflammation.[123] Subsequent studies have used antibody targeting of P-selectin, VCAM, and ICAM for studies of induced inflammation, acute cardiac transplant rejection, and atherosclerosis.[124,125] Microbubbles were retained in the mouse cremaster muscle and kidney with induced inflammation compared to controls in nonstimulated normal muscle and in P-selectin-deficient mice.[124] Acoustically-reflective liposomes targeted to ICAM-1 qualitatively showed acoustic image enhancement *in vivo* using transvascular and IVUS.[126] Increasingly sophisticated ligand systems have been shown to enable capture of microbubbles over a wide range of flow rates,[73,127,128] facilitating rapid and firm capture.

Thrombus

The development of contrast agents that enhance the detection of blood clots that are associated with stroke, myocardial infarction, and deep-vein thrombosis has been an important goal. *In vitro* targeting of thrombi was performed by Lanza and colleagues[3] using fibrin-targeted nanoparticles. Using antifibrinogen-targeted echogenic liposomes, thrombi were visible with epicardial and transthoracic ultrasound.[129]

Angiogenesis

Many receptors have recently been shown to be upregulated on angiogenic and metastatic endothelial cells.[130] Integrins have been widely evaluated for targeting of imaging agents, drugs, and particles to the tumor endothelium,

with $\alpha_v\beta_3$ perhaps receiving the greatest attention.[131,132] Targeting of microbubbles to glial tumors' integrins via echistatin has been demonstrated[133] and to a Matrigel model system in a study by Stieger.[134] The peptide arginine-arginine-leucine was shown to selectively target microbubbles to angiogenic tumor vasculature by a mechanism that remains unknown.[135] Antibodies to VEGF-R2 have been attached to microbubbles and used to selectively image malignant tumors in a study by Willmann and colleagues[136] and Lee and colleagues.[137] Dual imaging with ligands directed to both VEGF-R2 and the $\alpha_v\beta_3$ integrin increased the targeted agent signal compared with the singly labeled microbubbles.[20]

SAFETY

The complement proteins are an integral part of the innate immune system, which is the main line of defense in detecting and removing foreign pathogens in the body. The immunity pathways converge on the complement protein C3 that is converted to the fragments C3b and C3a by C3 convertase.[138] Normally, these fragments are degraded and recycled by complement-control elements to maintain homeostasis. The complement system is activated when C3b binds to the surface of a foreign particle. Immobilized C3b can be recognized by phagocytic cells, and it can interact with the other complement proteins to stimulate humoral immunity and form the membrane attack complex. The C3b fragment is a sticky molecule; it contains an unstable thioester bond that binds to an array of nucleophilic groups.[139] This poses a significant challenge for engineering therapeutic devices for injection or transplantation. Surface passivation with methyl-terminated poly(ethylene glycol) (mPEG) chains has been a major advance in biomaterials science. On liposomes, for example, the mPEG brush has been shown to significantly increase particle circulation half-life.[140]

Interestingly, the prolonged lifetimes of sterically protected particles in the circulation may not result directly from reduced protein adsorption.[141–145] Opsonization of sterically protected particles often does occur as exemplified by complement activation by long-circulating liposomes.[146] For example, Doxil® (Ortho Biotech) has been shown to produce significant complement activation in human serum *in vitro*, where incubation of Doxil increased complement protein complex SC5b-9 levels 100 to 200% over control in 7 of 10 different normal human sera.[146] This result supports the notion that the negative charge associated with the phosphate group in DSPE–mPEG2000 may play a critical role in complement activation. The reason that stealth liposomes remain long circulating while they are associated with complement activation is not fully known. One hypothesis is that inaccessible complement fixation on PEG-bearing liposomes prevents ligation to complement receptors.[147] For liposomes, methylation of the phosphate oxygen of phospholipid-mPEG conjugate, and hence the removal of the negative charge, totally prevented complement activation.[144]

For microbubbles, there is also substantial evidence that charged lipids play a role in complement activation. Preferential complement attachment has been shown to lipid-shelled microbubbles with a net negative charge[29] and those exposing biotin or RGD.[66,67] Complement C3 has also been shown to bind to albumin-encapsulated microbubbles, mediating adherence of the microbubble to the vascular endothelium.[26] Adverse reactions to ultrasound contrast agents have been rare in human studies; these have typically been transient and mild.[148] A small number of serious reactions have been reported, including severe hypotension, bradycardia, anaphylactic shock, and fatal outcome in patients undergoing contrast echocardiography. While these observations must be viewed in the light of millions of examinations, at this writing the European Medicine Agency (EMEA) and United States FDA have recently taken steps to limit the use of microbubbles or recommend cardiac monitoring in a small subset of patients.[148,149] At the current time, based on new reports[150] these changes are not expected to substantially influence the field of ultrasound contrast imaging.

Safety of Targeted Agents

Decorating microbubbles with targeting ligands—such as proteins, peptides, or metabolites—could further present chemical groups that bind to C3b and trigger immune activation. The same holds for other colloidal constructs used as imaging contrast agents. Clearly, avoidance of an immunogenic response is desirable for targeted contrast agents, not just to minimize hypersensitivity reactions but also to enable long enough circulation persistence for accumulation at the target. Ideally, the targeting ligand would be hidden from the milieu until the contrast agent reaches the target site, where it is exposed for binding and through multiple ligand-receptor interactions results in adhesion. The unique properties of microbubbles (expansion and contraction in response to an ultrasound field) have been shown to facilitate a stealth ligand.[66,67]

Safety of Insonified Contrast Agents

Ultrasound contrast imaging, thus far used clinically only without a targeting ligand, has been widely shown to be safe and efficacious, with no evidence of cavitation-related biological effects in humans.[151] *In vitro*, traveling shock waves, fluid shear waves, and liquid jets have been observed, impinging on walls or the cell monolayer.[80,152,153] Such effects are assumed to be exploitable for microbubble-induced drug and gene delivery *in vivo*.[154–156] These effects are a function of frequency, with a dependence on frequency that is greater than that predicted by the mechanical index and also increase with transmitted pressure.[157] Direct observations of microbubble oscillation within small blood vessels and models for constrained microbubble oscillation have been reported only recently, where the expansion of microbubbles was reported to be diminished within vessels with a diameter on the order of 15 μm or less.[78,111]

CHALLENGES AND LIMITATIONS

Microbubbles, which are the most echogenic of ultrasound contrast agents, are large and therefore constrained to the intravascular space. This limits the type of receptor molecules that can be targeted and restricts molecular imaging to endothelial cell surface phenotypes. However, there are several important vascular markers that are readily accessible to microbubble targeting, and methods are underway to improve the echogenicity and signal detection of nanoparticle contrast agents. Challenges for ultrasound molecular imaging include enhancing target accumulation and improving the delineation of signals from free and bound microbubbles. More work needs to be done to better understand the *in vivo* fate of targeted microbubbles and the associated bioeffects when insonified by ultrasound. It should also be mentioned that through microbubble-induced vessel permeabilization, ultrasound may provide a means of facilitating other molecular imaging modalities by allowing molecular probes to reach their extravascular target.

CONCLUSIONS AND FUTURE DIRECTIONS

Ultrasound molecular imaging is an emerging field that is enabling real-time, *in vivo* imaging of several vascular disease processes through longitudinal studies. Research on the fundamental physicochemistry and acoustic response of microbubbles has led to revolutionary advances in the rational design of microbubbles and ultrasound systems that better detect their signature echoes. Commercial systems are currently available, and ultrasound now presents a practical, economical, and effective means of molecular imaging. Yet the field currently is restricted to animal models of human disease. Several new microbubble constructs, targeting strategies, comprehensive scanner systems and imaging protocols are currently under development to expand this technology to the clinical arena.

REFERENCES

1. Couture O, Bevan PD, Cherin E, et al. Investigating perfluorohexane particles with high-frequency ultrasound. Ultrasound Med Biol 2006;32:73–82.
2. Lanza GM, Wallace KD, Scott MJ, et al. A novel site-targeted ultrasonic contrast agent with broad biomedical application. Circulation 1996;94:3334–40.
3. Lanza GM, Wallace KD, Fischer SE, et al. High-frequency ultrasonic detection of thrombi with a targeted contrast system. Ultrasound Med Biol 1997;23:863–70.
4. Wickline SA, Lanza GM. Nanotechnology for molecular imaging and targeted therapy. Circulation 2003;107:1092–5.
5. Correas JM, Quay SD. EchoGen(TM) emulsion: a new ultrasound contrast agent based on phase shift colloids. Clin Radiol 1996;51:11–4.
6. Rapoport N, Gao ZG, Kennedy A. Multifunctional nanoparticles for combining ultrasonic tumor imaging and targeted chemotherapy. J Natl Cancer Inst 2007;99:1095–106.
7. Alkan-Onyuksel H, Demos SM, Lanza GM, et al. Development of inherently echogenic liposomes as an ultrasonic contrast agent. J Pharm Sci 1996;85:486–90.
8. Huang SL, Hamilton AJ, Nagaraj A, et al. Improving ultrasound reflectivity and stability of echogenic liposomal dispersions for use as targeted ultrasound contrast agents. J Pharm Sci 2001;90:1917–26.
9. Huang SL, Hamilton AJ, Pozharski E, et al. Physical correlates of the ultrasonic reflectivity of lipid dispersions suitable as diagnostic contrast agents. Ultrasound Med Biol 2002;28:339–48.
10. Marik J, Tartis MS, Zhang H, et al. Long-circulating liposomes radiolabeled with [18F]fluorodipalmitin ([18F]FDP). Nucl Med Biol 2007;34:165–71.
11. Zhang H, Kusunose J, Kheirolomoom A, et al. Dynamic imaging of arginine-rich heart-targeted vehicles in a mouse model. Biomaterials 2008;29:1976–88.
12. Parker KJ, Tuthill TA, Lerner RM, Violante MR. A particulate contrast agent with potential for ultrasound imaging of liver. Ultrasound Med Biol 1987;13:555–66.
13. Liu J, Levine AL, Mattoon JS, et al. Nanoparticles as image enhancing agents for ultrasonography. Phys Med Biol 2006;51:2179–89.
14. Goldsmith H, Mason SG. Axial migration of particles in Poiseuille flow. Nature 1961;190:1095–6.
15. Feinstein SB, Shah PM, Bing RJ, et al. Microbubble dynamics visualized in the intact capillary circulation. J Am Coll Cardiol 1984;4:595–600.
16. Keller MW, Segal SS, Kaul S, Duling B. The behavior of sonicated albumin microbubbles within the microcirculation—a basis for their use during myocardial contrast echocardiography. Circ Res 1989;65:458–67.
17. Lindner JR, Song J, Jayaweera AR, et al. Microvascular rheology of definity microbubbles after intra-arterial and intravenous administration. J Am Soc Echocardiogr 2002;15:396–403.

18. Braide M, Rasmussen H, Albrektsson A, Bagge U. Microvascular behavior and effects of Sonazoid microbubbles in the cremaster muscle of rats after local administration. J Ultrasound Med 2006;25:883–90.
19. Tartis M, K D, Zheng H, et al. Dynamic microPET imaging of ultrasound contrast agents and lipid delivery. J Control Release 2008. [In press]
20. Willmann JK, L A, Paulmurugan R, et al. Dual-targeted contrast agent for ultrasonic assessment of tumor angiogenesis *in vivo*. Radiology 2008. [In press]
21. Killam AL, Mehlhaff PM, Zavorskas PA, et al. Tissue distribution of I-125-labeled albumin in rats, and whole blood and exhaled elimination kinetics of octafluoropropane in anesthetized canines, following intravenous administration of OPTISON (R) (FS069). Int J Toxicol 1999;18:49–63.
22. Walday P, Tolleshaug H, Gjoen T, et al. Biodistributions of air-filled albumin microspheres in rats and pigs. Biochem J 1994;299:437–43.
23. Lindner JR, Dayton PA, Coggins MP, et al. Noninvasive imaging of inflammation by ultrasound detection of phagocytosed microbubbles. Circulation 2000;102:531–8.
24. Lindner JR, Coggins MP, Kaul S, et al. Microbubble persistence in the microcirculation during ischemia/reperfusion and inflammation is caused by integrin- and complement-mediated adherence to activated leukocytes. Circulation 2000;101:668–75.
25. Xie F, Tsutsui JM, Anderson D, et al. Detection of albumin microbubble adherence to aortic endothelium at different stages in the atherosclerotic process. J Am Coll Cardiol 2007;49:A167.
26. Anderson DR, Tsutsui JM, Xie F, et al. The role of complement in the adherence of microbubbles to dysfunctional arterial endothelium and atherosclerotic plaque. Cardiovasc Res 2007;73:597–606.
27. Yanagisawa K, Moriyasu F, Miyahara T, et al. Phagocytosis of ultrasound contrast agent microbubbles by Kupffer cells. Ultrasound Med Biol 2007;33:318–25.
28. Kindberg GM, Tolleshaug H, Roos N, Skotland T. Hepatic clearance of Sonazoid perfluorobutane microbubbles by Kupffer cells does not reduce the ability of liver to phagocytose or degrade albumin microspheres. Cell Tissue Res 2003;312:49–54.
29. Fisher NG, Christiansen JP, Klibanov A, et al. Influence of microbubble surface charge on capillary transit and myocardial contrast enhancement. J Am Coll Cardiol 2002;40:811–9.
30. Kvale S, Jakobsen HA, Asbjornsen OA, Omtveit T. Size fractionation of gas-filled microspheres by flotation. Sep Technol 1996;6:219–26.
31. Ganan-Calvo AM, Gordillo JM. Perfectly monodisperse microbubbling by capillary flow focusing. Phys Rev Lett 2001;87.
32. Talu E, Lozano MM, Powell RL, et al. Long-term stability by lipid coating monodisperse microbubbles formed by a flow-focusing device. Langmuir 2006;22:9487–90.
33. Xu JH, Li SW, Wang YJ, Luo GS. Controllable gas-liquid phase flow patterns and monodisperse microbubbles in a microfluidic T-junction device. Appl Phys Lett 2006;88.
34. Bohmer MR, Schroeders R, Steenbakkers JAM, et al. Preparation of monodisperse polymer particles and capsules by ink-jet printing. Colloids Surf A Physicochem Eng Asp 2006;289:96–104.
35. Farook U, Stride E, Edirisinghe MJ, Moaleji R. Microbubbling by co-axial electrohydrodynamic atomization. Med Biol Eng Comput 2007;45:781–9.
36. Wheatley MA, Schrope B, Shen P. Contrast agents for diagnostic ultrasound—development and evaluation of polymer-coated microbubbles. Biomaterials 1990;11:713–7.
37. Schneider M, Arditi M, Barrau MB, et al. Br1—a new ultrasonographic contrast agent based on sulfur hexafluoride-filled microbubbles. Invest Radiol 1995;30:451–7.
38. Bjerknes K, Braenden JU, Braenden JE, et al. Air-filled polymeric microcapsules from emulsions containing different organic phases. J Microencapsul 2001;18:159–71.
39. Narayan P, Wheatley MA. Preparation and characterization of hollow microcapsules for use as ultrasound contrast agents. Polym Eng Sci 1999;39:2242–55.
40. Schmidt W, Roessling G. Novel manufacturing process of hollow polymer microspheres. Chem Eng Sci 2006; 61:4973–81.
41. Cavalieri F, El Hamassi A, Chiessi E, Paradossi G. Stable polymeric microballoons as multifunctional device for biomedical uses: synthesis and characterization. Langmuir 2005;21:8758–64.
42. Leong-Poi H, Song J, Rim SJ, et al. Influence of microbubble shell properties on ultrasound signal: implications for low-power perfusion imaging. J Am Soc Echocardiogr 2002;15:1269–76.
43. Bloch SH, Wan M, Dayton PA, Ferrara KW. Optical observation of lipid- and polymer-shelled ultrasound microbubble contrast agents. Appl Phys Lett 2004;84:631–3.
44. Hunter RJ. Foundations of colloid science. Vol I. Oxford: Oxford University Press;1986.
45. Duncan PB, Needham D. Test of the Epstein-Plesset model for gas microparticle dissolution in aqueous media: effect of surface tension and gas undersaturation in solution. Langmuir 2004;20:2567–78.
46. Epstein PS, Plesset MS. On the stability of gas bubbles in liquid-gas solutions. J Chem Phys 1950;18:1505–9.
47. Kabalnov A, Klein D, Pelura T, et al. Dissolution of multicomponent microbubbles in the bloodstream: 1. Theory. Ultrasound Med Biol 1998;24:739–49.
48. Kabalnov A, Bradley J, Flaim S, et al. Dissolution of multicomponent microbubbles in the bloodstream: 2. Experiment. Ultrasound Med Biol 1998;24:751–60.
49. Kabalnov AS, Makarov KN, Shcherbakova OV. Solubility of fluorocarbons in water as a key parameter determining fluorocarbon emulsion stability. J Fluor Chem 1990;50:271–84.
50. Crane JM, Hall SB. Rapid compression transforms interfacial monolayers of pulmonary surfactant. Biophys J 2001;80:1863–72.
51. Borden MA, Martinez GV, Ricker J, et al. Lateral phase separation in lipid-coated microbubbles. Langmuir 2006;22:4291–7.
52. Borden MA, Longo ML. Dissolution behavior of lipid monolayer-coated, air-filled microbubbles: effect of lipid hydrophobic chain length. Langmuir 2002;18:9225–33.
53. Feinstein SB, Cheirif J, Tencate FJ, et al. Safety and efficacy of a new transpulmonary ultrasound contrast agent—initial multicenter clinical-results. J Am Coll Cardiol 1990;16:316–24.
54. Korpanty G, Grayburn PA, Shohet RV, Brekken RA. Targeting vascular endothelium with avidin microbubbles. Ultrasound Med Biol 2005;31:1279–83.
55. Frenkel PA, Chen SY, Thai T, et al. DNA-loaded albumin microbubbles enhance ultrasound-mediated transfection *in vitro*. Ultrasound Med Biol 2002;28:817–22.
56. Lentacker I, De Geest BG, Vandenbroucke RE, et al. Ultrasound-responsive polymer-coated microbubbles that bind and protect DNA. Langmuir 2006;22:7273–8.
57. Dayton PA, Morgan KE, Klibanov AL, et al. Optical and acoustical observations of the effects of ultrasound on contrast agents. IEEE Trans Ultrason Ferroelectr Freq Control 1999;46:220–32.
58. Klibanov AL. Ultrasound contrast agents: development of the field and current status. Top Curr Chem 2002;222:73–106.
59. Kim DH, Klibanov AL, Needham D. The influence of tiered layers of surface-grafted poly(ethylene glycol) on receptor-ligand-mediated adhesion between phospholipid monolayer-stabilized microbubbles and coated class beads. Langmuir 2000;16:2808–17.
60. Kim DH, Costello MJ, Duncan PB, Needham D. Mechanical properties and microstructure of polycrystalline phospholipid monolayer shells: novel solid microparticles. Langmuir 2003;19:8455–66.
61. Borden MA, Longo ML. Oxygen permeability of fully condensed lipid monolayers. J Phys Chem B 2004;108:6009–16.
62. Pu G, Borden MA, Longo ML. Collapse and shedding transitions in binary lipid monolayers coating microbubbles. Langmuir 2006;22:2993–9.
63. Borden MA, Kruse DE, Caskey CF, et al. Influence of lipid shell physicochemical properties on ultrasound-induced microbubble destruction. IEEE Trans Ultrason Ferroelectr Freq Control 2005;52:1992–2002.

64. Borden MA, Pu G, Runner GJ, Longo ML. Surface phase behavior and microstructure of lipid/PEG-emulsifier monolayer-coated microbubbles. Colloids Surf B Biointerfaces 2004;35:209–23.
65. Pu G, Longo ML, Borden MA. Effect of microstructure on molecular oxygen permeability through condensed phospholipid monolayers. J Am Chem Soc 2005;127:6524–5.
66. Borden MA, Sarantos MR, Stieger SM, et al. Ultrasound radiation force modulates ligand availability on targeted contrast agents. Mol Imaging 2006;5:139–47.
67. Borden MA, Zhang H, Gillies RJ, et al. A stimulus-responsive contrast agent for ultrasound molecular imaging. Biomaterials 2007. [In press]
68. Jeppesen C, Wong JY, Kuhl TL, et al. Impact of polymer tether length on multiple ligand-receptor bond formation. Science 2001;293:465–8.
69. Lin JJ, Silas JA, Bermudez H, et al. The effect of polymer chain length and surface density on the adhesiveness of functionalized polymersomes. Langmuir 2004;20:5493–500.
70. Chan WC, White PD. Fmoc solid phase peptide synthesis: a practical approach. New York: Oxford University Press; 2000.
71. Klibanov AL. Ligand-carrying gas-filled microbubbles: ultrasound contrast agents for targeted molecular imaging. Bioconjug Chem 2005;16:9–17.
72. Lanza GM, Wickline SA. Targeted ultrasonic contrast agents for molecular imaging and therapy. Prog Cardiovasc Dis 2001;44:13–31.
73. Klibanov AL, Rychak JJ, Yang WC, et al. Targeted ultrasound contrast agent for molecular imaging of inflammation in high-shear flow. Contrast Media Mol Imaging 2006;1:259–66.
74. Shchukin DG, Kohler K, Mohwald H, Sukhorukov GB. Gas-filled polyelectrolyte capsules. Angew Chem Int Ed Engl 2005;44:3310–4.
75. Borden MA, Caskey CF, Little E, et al. DNA and polylysine adsorption and multilayer construction onto cationic lipid-coated microbubbles. Langmuir 2007;23:9401–8.
76. Klibanov AL, Ferrara KW, Hughes MS, et al. Direct video microscopic observation of the dynamic effects of medical ultrasound on ultrasound contrast microspheres. Invest Radiol 1998;33:863–70.
77. Dayton PA, Morgan KE, Klibanov ALS, et al. A preliminary evaluation of the effects of primary and secondary radiation forces on acoustic contrast agents. IEEE Trans Ultrason Ferroelectr Freq Control 1997;44:1264–77.
78. Caskey CF, Stieger SM, Qin S, et al. Direct observations of ultrasound microbubble contrast agent interaction with the microvessel wall. J Acoust Soc Am 2007;122:1191–200.
79. de Jong N, Frinking PJA, Bouakaz A, et al. Optical imaging of contrast agent microbubbles in an ultrasound field with a 100-MHz camera. Ultrasound Med Biol 2000;26:487–92.
80. Prentice P, Cuschieri A, Dholakia K, et al. Membrane disruption by optically controlled microbubble cavitation. Nat Phys 2005;1:107–10.
81. Chomas JE, Dayton PA, May D, et al. Optical observation of contrast agent destruction. Appl Phys Lett 2000;77:1056–8.
82. Rayleigh L. On the pressure developed in a liquid during the collapse of a spherical cavity. Philos Mag 1917;34:94–8.
83. Vokurka K. On Rayleigh model of a freely oscillating bubble. 1. Basic relations. Czech J Phys 1985;35:28–40.
84. Plesset MS, Prosperetti A. Bubble dynamics and cavitation. Annu Rev Fluid Mech 1977;9:145–85.
86. Putterman S, Evans PG, Vazquez G, Weninger K. Cavitation science—is there a simple theory of sonoluminescence? Nature 2001;409:782–3.
87. Prosperetti A. Bubble dynamics—a review and some recent results. Appl Sci Res 1982;38:145–64.
88. Miller DL. Ultrasonic-detection of resonant cavitation bubbles in a flow tube by their 2nd-harmonic emissions. Ultrasonics 1981;19:217–24.
89. Prosperetti A, Lezzi A. Bubble dynamics in a compressible liquid. 1. 1st-order theory. J Fluid Mech 1986;168:457–78.
90. Prosperetti A. The equation of bubble dynamics in a compressible liquid. Phys Fluids 1987;30:3626–8.
91. Lezzi A, Prosperetti A. Bubble dynamics in a compressible liquid. 2. 2nd-order theory. J Fluid Mech 1987;185:289–321.
92. Keller JB, Kolodner II. Damping of underwater explosion bubble oscillations. J Appl Phys 1956;27:1152–61.
93. Keller JB, Miksis M. Bubble oscillations of large-amplitude. J Acoust Soc Am 1980;68:628–33.
94. Prosperetti A, Crum LA, Commander KW. Nonlinear bubble dynamics. J Acoust Soc Am 1988;83:502–14.
95. Trilling L. The collapse and rebound of a gas bubble. J Appl Phys 1952;23:14–7.
96. Brenner CE. Cavitation and bubble dynamics. Oxford: Oxford University;1995.
97. Gilmore FR. The growth or collapse of a spherical bubble in a viscous compressible liquid. In: Hydrodynamics laboratory. Pasadena (CA): California Institute Technology;1952.
98. Barber BP, Hiller RA, Lofstedt R, et al. Defining the unknowns of sonoluminescence. Phys Rep 1997;281:65–143.
99. Lofstedt R, Weninger K, Putterman S, Barber BP. Sonoluminescing bubbles and mass diffusion. Phys Rev E 1995;51: 4400–10.
100. Chomas JE, Dayton P, Allen J, et al. Mechanisms of contrast agent destruction. IEEE Trans Ultrason Ferroelectr Freq Control 2001;48:232–48.
101. Morgan KE, Allen JS, Dayton PA, et al. Experimental and theoretical evaluation of microbubble behavior: effect of transmitted phase and bubble size. IEEE Trans Ultrason Ferroelectr Freq Control 2000;47:1494–509.
102. de Jong N, Cornet R, Lancee CT. Higher harmonics of vibrating gas-filled microspheres. 1. Simulations. Ultrasonics 1994;32:447–53.
103. de Jong N, Cornet R, Lancee CT. Higher harmonics of vibrating gas-filled microspheres. 2. Measurements. Ultrasonics 1994;32:455–9.
104. de Jong N, Hoff L. Ultrasound scattering properties of Albunex microspheres. Ultrasonics 1993;31:175–81.
105. de Jong N, Hoff L, Skotland T, Bom N. Absorption and scatter of encapsulated gas filled microspheres—theoretical considerations and some measurements. Ultrasonics 1992;30:95–103.
106. Church CC. The effects of an elastic solid-surface layer on the radial pulsations of gas-bubbles. J Acoust Soc Am 1995;97:1510–21.
107. Hoff L, Sontum PC, Hovem JM. Oscillations of polymeric microbubbles: effect of the encapsulating shell. J Acoust Soc Am 2000;107:2272–80.
108. Ory E, Yuan H, Prosperetti A, et al. Growth and collapse of a vapor bubble in a narrow tube. Phys Fluids 2000;12:1268–77.
109. Yuan H, Oguz HN, Prosperetti A. Growth and collapse of a vapor bubble in a small tube. Int J Heat Mass Transf 1999; 42:3643–57.
110. Hu YT, Qin SP, Hu T, et al. Asymmetric oscillation of cavitation bubbles in a microvessel and its implications upon mechanisms of clinical vessel injury in shock-wave lithotripsy. Int J Nonlinear Mech 2005;40:341–50.
111. Qin SP, Ferrara KW. Acoustic response of compliable microvessels containing ultrasound contrast agents. Phys Med Biol 2006;51:5065–88.
112. Qin SP, Ferrara KW. The natural frequency of nonlinear oscillation of ultrasound contrast agents in microvessels. Ultrasound Med Biol 2007;33:1140–8.
113. Sassaroli E, Hynynen K. Resonance frequency of microbubbles in small blood vessels: a numerical study. Phys Med Biol 2005;50:5293–305.
114. Sassaroli E, Hynynen K. On the impact of vessel size on the threshold of bubble collapse. Appl Phys Lett 2006;89:123901.
115. Ye T, Bull JL. Microbubble expansion in a flexible tube. J Biomech Eng 2006;128:554–63.

116. Oguz HN, Prosperetti A. The natural frequency of oscillation of gas bubbles in tubes. J Acoust Soc Am 1998;103:3301–8.
117. Caskey CF, Kruse DE, Dayton PA, et al. Microbubble oscillation in tubes with diameters of 12, 25, and 195 microns. Appl Phys Lett 2006;88:033902.
118. Dayton PA, Chomas JE, Lum AFH, et al. Optical and acoustical dynamics of microbubble contrast agents inside neutrophils. Biophys J 2001;80:1547–56.
119. Zhao S, Kruse DE, Ferrara KW, Dayton PA. Selective imaging of adherent targeted ultrasound contrast agents. Phys Med Biol 2007;52:2055–72.
120. Lum AFH, Borden MA, Dayton PA, et al. Ultrasound radiation force enables targeted deposition of model drug carriers loaded on microbubbles. J Control Release 2006;111:128–34.
121. Nakashima Y, Raines EW, Plump AS, et al. Upregulation of VCAM-1 and ICAM-1 at atherosclerosis-prone sites on the endothelium in the apoE-deficient mouse. Arterioscler Thromb Vasc Biol 1998;18:842–51.
122. Jian-Guo G, Ming C, Kuo-Chen C. P-selectin cell adhesion molecule in inflammation, thrombosis, cancer growth and metastasis. Curr Med Chem 2004;11:2153–60.
123. Christiansen JP, Leong-Poi H, Klibanov AL, et al. Noninvasive imaging of myocardial reperfusion injury using leukocyte-targeted contrast echocardiography. Circulation 2002;105:1764–7.
124. Lindner JR, Song J, Christiansen J, et al. Ultrasound assessment of inflammation and renal tissue injury with microbubbles targeted to P-selectin. Circulation 2001;104:2107–12.
125. Weller GER, Lu E, Csikari MM, et al. Ultrasound imaging of acute cardiac transplant rejection with microbubbles targeted to intercellular adhesion molecule-1. Circulation 2003;108:218–24.
126. Hamilton AJ, Huang SL, Warnick D, et al. Intravascular ultrasound molecular Imaging of atheroma components *in vivo*. J Am Coll Cardiol 2004;43:453–60.
127. Kaufmann BA, Lewis C, Xie A, et al. Detection of recent myocardial ischaemia by molecular imaging of P-selectin with targeted contrast echocardiography. Eur Heart J 2007;28:2011–7.
128. Kaufmann BA, Sanders JM, Davis C, et al. Molecular imaging of inflammation in atherosclerosis with targeted ultrasound detection of vascular cell adhesion molecule-1. Circulation 2007;116:276–84.
129. Hamilton A, Huang SL, Warnick D, et al. Left ventricular thrombus enhancement after intravenous injection of echogenic immunoliposomes—studies in a new experimental model. Circulation 2002;105:2772–8.
130. Ruoslahti E. Vascular zip codes in angiogenesis and metastasis. Biochem Soc Trans 2004;32:397–402.
131. Varner JA, Cheresh DA. Integrins and cancer. Curr Opin Cell Biol 1996;8:724–30.
132. Ruoslahti E. The RGD story: a personal account. Matrix Biol 2003;22:459–65.
133. Ellegala DB, Poi HL, Carpenter JE, et al. Imaging tumor angiogenesis with contrast ultrasound and microbubbles targeted to $\alpha_v\beta_3$. Circulation 2003;108:336–41.
134. Stieger SM, Dayton PA, Borden MA, et al. Imaging of angiogenesis using Cadence™ contrast pulse sequencing and targeted contrast agents. Contrast Media Mol Imaging 2008;3:9–18.
135. Weller GER, Wong MKK, Modzelewski RA, et al. Ultrasonic imaging of tumor angiogenesis using contrast microbubbles targeted via the tumor-binding peptide arginine-arginine-leucine. Cancer Res 2005;65:533–9.
136. Willmann JK, Paulmurugan R, Chen K, et al. Ultrasonic imaging of tumor angiogenesis with contrast microbubbles targeted to vascular endothelial growth factor receptor 2 in mice. Radiology 2008;246:508–18.
137. Lee DJ, Lyshchik A, Huamani J, et al. Relationship between retention of a vascular endothelial growth factor receptor 2 (VEGFR2)-targeted ultrasonographic contrast agent and the level of VEGFR2 expression in an *in vivo* breast cancer model. J Ultrasound Med 2008;27:855–66.
138. Sahu A, Lambris JD. Structure and biology of complement protein C3, a connecting link between innate and acquired immunity. Immunol Rev 2001;180:35–48.
139. Janssen BJC, Huizinga EG, Raaijmakers HCA, et al. Structures of complement component C3 provide insights into the function and evolution of immunity. Nature 2005;437:505–11.
140. Klibanov AL, Maruyama K, Torchilin VP, Huang L. Amphipathic polyethyleneglycols effectively prolong the circulation time of liposomes. FEBS Lett 1990;268:235–7.
141. Moghimi SM, Muir IS, Illum L, et al. Coating particles with a block co-polymer (poloxamine-908) suppresses opsonization but permits the activity of dysopsonins in the serum. Biochim Biophys Acta 1993;1179:157–65.
142. Price ME, Cornelius RM, Brash JL. Protein adsorption to polyethylene glycol modified liposomes from fibrinogen solution and from plasma. Biochim Biophys Acta 2001;1512:191–205.
143. Moghimi SM, Szebeni J. Stealth liposomes and long circulating nanoparticles: critical issues in pharmacokinetics, opsonization and protein-binding properties. Prog Lipid Res 2003;42:463–78.
144. Moghimi SM, Hamad I, Andresen TL, et al. Methylation of the phosphate oxygen moiety of phospholipid-methoxy(polyethylene glycol) conjugate prevents PEGylated liposome-mediated complement activation and anaphylatoxin production. FASEB J 2006;20:2591–3.
145. Moghimi SM, Hamad I, Bunger R, et al. Activation of the human complement system by cholesterol-rich and pegylated liposomes—modulation of cholesterol-rich liposome-mediated complement activation by elevated serum LDL and HDL levels. J Liposome Res 2006;16:167–74.
146. Szebeni J, Baranyi L, Savay S, et al. Role of complement activation in hypersensitivity reactions to Doxil and HYNIC PEG liposomes: experimental and clinical studies. J Liposome Res 2002;12:165–72.
147. Wilkinson BJ, Peterson PK, Quie PG. Cryptic peptidoglycan and the antiphagocytic effect of the Staphylococcus aureus capsule: model for the antiphagocytic effect of bacterial cell surface polymers. Infect Immun 1979;23:502–8.
148. Correas JM, Bridal L, Lesavre A, et al. Ultrasound contrast agents: properties, principles of action, tolerance, and artifacts. Eur Radiol 2001;11:1316–28.
149. Torzilli G. Adverse effects associated with SonoVue use. Expert Opin Drug Saf 2005;4:399–401.
150. Available at: http://www.radiopharm .com/ News_03132008 .html.
151. Quaia E. Microbubble ultrasound contrast agents: an update. Eur Radiol 2007;17:1995–2008.
152. Lauterborn W, Ohl CD. Cavitation bubble dynamics. Ultrason Sonochem 1997;4:65–75.
153. Wolfrum B, Mettin R, Kurz T, Lauterborn W. Observations of pressure-wave-excited contrast agent bubbles in the vicinity of cells. Appl Phys Lett 2002;81:5060–2.
154. Chen S, Ding J-H, Bekeredjian R, et al. Efficient gene delivery to pancreatic islets with ultrasonic microbubble destruction technology. Proc Natl Acad Sci U S A 2006;103:8469–74.
155. Choi JJ, Pernot M, Brown TR, et al. Spatio-temporal analysis of molecular delivery through the blood-brain barrier using focused ultrasound. Phys Med Biol 2007;52:5509–30.
156. Hynynen K, McDannold N, Sheikov NA, et al. Local and reversible blood-brain barrier disruption by noninvasive focused ultrasound at frequencies suitable for trans-skull sonications. Neuroimage 2005;24:12–20.
157. Stieger SM, Caskey CF, Adamson RH, et al. Enhancement of vascular permeability with low-frequency contrast-enhanced ultrasound in the chorioallantoic membrane model. Radiology 2007;243:112–21.
158. Guy CT, Cardiff RD, Muller WJ. Induction of mammary-tumors by expression of polyomavirus middle T-oncogene—a transgenic mouse model for metastatic disease. Mol Cell Biol 1992;12:954–61.